Inorganic Chemistry

Article

pubs.acs.org/IC

Synthesis and Characterization of Hypoelectronic Tantalaboranes: Comparison of the Geometric and Electronic Structures of $[(Cp^*TaX)_2B_5H_{11}]$ (X = Cl, Br, and I)

K. Geetharani,[†] Bellie Sundaram Krishnamoorthy,[‡] Samia Kahlal,[‡] Shaikh M. Mobin,[§] Jean-François Halet,*[,‡] and Sundargopal Ghosh*[,†]

[†]Department of Chemistry, Indian Institute of Technology Madras, Chennai 600 036, India

[‡]Institut des Sciences Chimiques de Rennes, UMR 6226 CNRS-Université de Rennes 1, Avenue du Général Leclerc, Rennes Cedex, France

[§]National Single Crystal X-ray Diffraction Facility, Indian Institute of Technology Bombay, Mumbai 400 076, India

Supporting Information

ABSTRACT: Mild thermolysis of tantalaborane $[(Cp^*Ta)_2B_5H_{11}]$, **1** ($Cp^* = \eta^5$-C_5Me_5) in presence of halogen sources affords the open cage clusters $[(Cp^*TaX)_2B_5H_{11}]$, **2**–**4** (**2**: X = Cl; **3**: X = Br; and **4**: X = I) in good yields. In contrast, the tetraborohydride cluster, $[(Cp^*Ta)_2B_4H_9(\mu\text{-}BH_4)]$, **5**, under the same reaction conditions forms the B–H substituted cluster $[(Cp^*Ta)_2B_4H_8I(\mu\text{-}BH_4)]$, **6**. All the new metallaboranes have been characterized by mass spectrometry, ^1H, ^{11}B, ^{13}C NMR spectroscopy, and elemental analysis, and the structural types were established by crystallographic analysis of clusters **3**, **4**, and **6**. Density functional theory (DFT) calculations at the BP86/TZ2P ZORA level reveal geometries in agreement with the structure determinations, large gaps between the highest occupied molecular orbital (HOMO) and the lowest unoccupied molecular orbital (LUMO) in accord with their stabilities. B3LYP-computed ^{11}B chemical shifts accurately reflect the experimentally measured shifts. Clusters **2**–**4** can be viewed as 7-sep 7-vertex *oblatoarachno* M_2B_5 clusters which can be generated from a 7-sep 9-vertex *oblatocloso* M_2B_7 cluster by removal of two equatorial boron atoms. Cluster **6** can be considered as an electron-deficient 6-sep 6-vertex *oblatoarachno* M_2B_4 cluster derived from an 8-vertex *oblatocloso* hexagonal bipyramidal cluster, in which BH_4^- anion is weakly bonded in a bidentate mode.

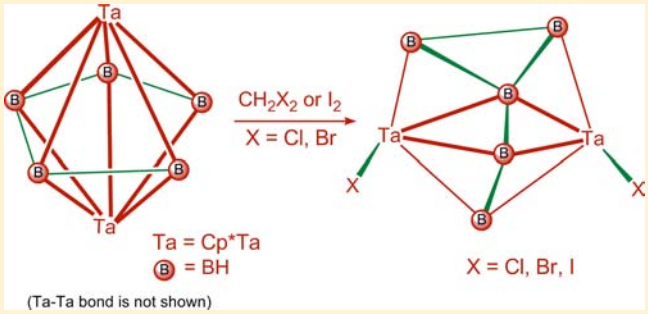

INTRODUCTION

Polyhedral boron-containing compounds show an extensive structural chemistry that exhibits clear interconnections with organometallic and other p-block-transition-element compounds.[1,2] However, limitations of synthetic methods have precluded systematic study of metallaboranes, and as a result their reactivity has remained largely unexplored relatively to that of organometallic compounds.[3−5] This changed significantly with the development of a general route to a class of metallaboranes in which the metal can be varied from Group 5–9.[6] Furthermore, the discovery of cluster electron counting rules and the isolobal principle, provide a solid foundation for understanding the inter relationships between structure and composition.[7,8]

In recent years, we have been exploring the reaction of group 5 monocyclopentadienylmetal chlorides with monoborane reagents as a general route to dimetallaboranes.[9−11] We have now begun to examine the systematic reaction chemistry of these clusters. As a result, thermal elimination reactions,[12a] as well as reactions with metal fragments,[12b,c] monoboranes,[12d] main group elements,[12e,f] and small organic molecules,[12g] have been described. In these reactions, the distinctive electronic contributions of metal and borane fragments to the cluster structure are seen to be expressed in the overall reactivity.[13] Here, we report the reactivity of tantalaboranes $[(Cp^*Ta)_2B_5H_{11}]$, **1**, ($Cp^* = \eta^5$-C_5Me_5) and $[(Cp^*Ta)_2B_4H_9(\mu\text{-}BH_4)]$, **5**, with different halogen sources and demonstrate in one case a change in geometry into open cage *oblatoarachno* tantalaboranes **2**–**4** and in another case a B–H substitution reaction. In addition, density functional theory (DFT) calculations are used to provide some insight into the nature of bonding and to confirm the number of bridging and terminal hydrogen atoms present in these metallaboranes.[14−17] Further, the ^{11}B and ^1H NMR chemical shift calculations provide a stringent test of the validity of the calculated electronic structures of these tantalaboranes.

Received: April 25, 2012
Published: September 10, 2012

Scheme 1. Synthesis of Tantalaboranes, 2−4

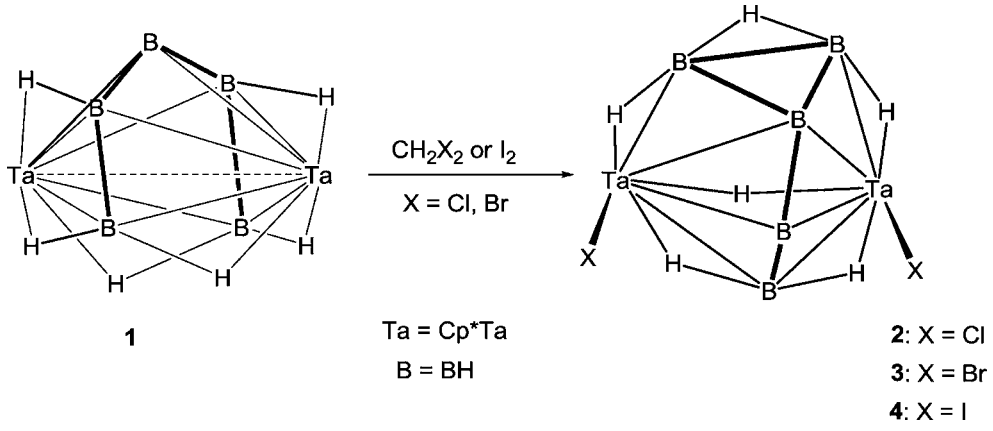

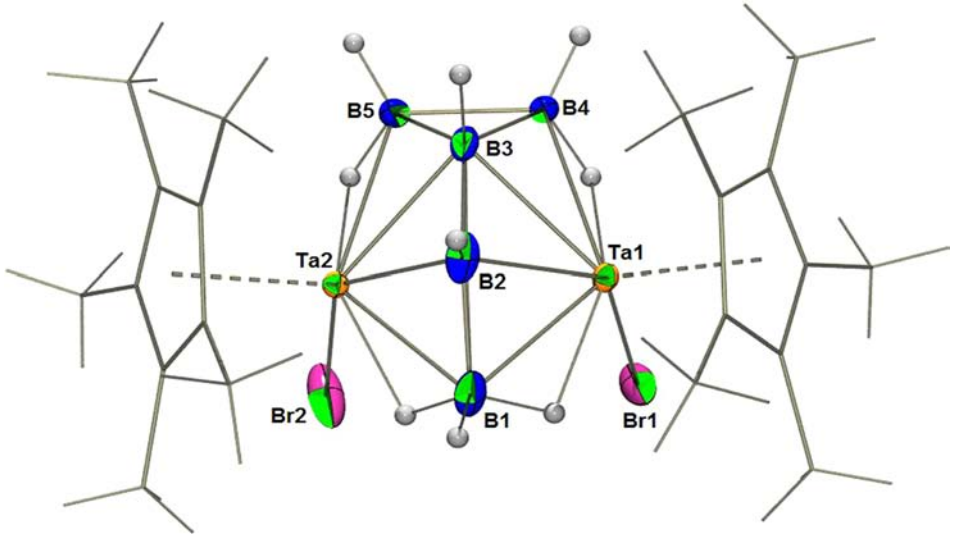

Figure 1. Molecular structure for $[(Cp^*TaBr)_2B_5H_{11}]$ **3**. Selected bond lengths (Å) and angles (deg): Ta1−Ta2 3.2280(4), Ta1−Br1 2.6212(9), Ta2−Br2 2.6018(9), Ta1−B2 2.274(9), Ta1−B3 2.424(8), Ta1−B1 2.405(10), Ta1−B4 2.426(8), Ta2−B2 2.253(8), Ta2−B1 2.419(9), Ta2−B3 2.427(8), Ta2−B5 2.425(9), B1−B2 1.716(15), B2−B3 1.705(14), B3−B5 1.770(14), B3−B4 1.789(14), B4−B5 1.816(11); B2−Ta1−B1 42.9(4), B(2)−Ta(1)−Ta(2) 44.3(2), B1−Ta1−Ta2 48.2(2), B4−Ta1−Ta2 73.24(19).

RESULTS AND DISCUSSION

Synthesis of Clusters 2−4. As shown in Scheme 1, clusters **2**−**4** were obtained in good yields from the reaction of **1** with excess of CH_2Cl_2, CH_2Br_2, and I_2, respectively. Although cluster **2** has been synthesized previously from the reaction of $[Cp^*TaCl_4]$, $[LiBH_4{\cdot}thf]$, and $[BH_3{\cdot}thf]$,[9] the isolated yield of **2** from this method is considerably higher than the route reported earlier. Details of spectroscopic and structural characterization of **3** and **4** using IR, ^1H, ^{11}B, ^{13}C NMR, mass spectrometry, and X-ray diffraction studies are given below.

Clusters **3** and **4** are isostructural with the Cl analogue, **2**.[9] The mass spectrum in the high m/z range shows a molecular ion peak at m/z 857 and 951 corroborating the composition of $C_{20}H_{41}Ta_2B_5Br_2$ and $C_{20}H_{41}Ta_2B_5I_2$ respectively. The ^{11}B NMR spectrum of **3** and **4** rationalizes the presence of four boron resonances in the ratio of 1:2:1:1, which collapsed into sharp singlet upon ^1H decoupling, indicating one terminal hydrogen atom on each boron atom. The ^1H and ^{13}C NMR spectra of **3** and **4**, measured at room temperature are consistent with its symmetrical structure. In particular, the ^1H NMR data reveal the presence of one kind of Cp* ligand, one Ta−H−Ta, one B−H−B and four Ta−H−B protons.

All the spectroscopic data are consistent with the solid-state structures which are shown in Figures 1 and 2. The clusters **3** and **4** may be seen as 7-vertex *oblatoarachno* M_2B_5 clusters,[18] which can indeed be derived from a 9-vertex *oblatocloso* M_2B_7 cluster encountered in $(Cp^*Re)_2B_7H_7$,[14] for example, by removal of two equatorial boron atoms. It has been shown that the latter was a hypoelectronic species with an *apparent* electron count of 7 skeletal electron pairs (sep) if the classical skeletal electron counting formalism (the Polyhedral Skeletal Electron Pair Theory, PSEPT)[19] is used. Counting the same way, clusters **2**−**4** lead to a count of either 5 sep ([−3 (Cp*TaX) × 2 + 2 (BH) × 5 + 1 (bridging H) × 6]/2) or 7 sep ([−1 (Cp*TaX) × 2 + 2 (BH) × 5 + 1 (bridging H) × 6]/2), depending on the geometrical and electronic features of the ML_4 fragment Cp*TaX (we will come back to this point later). It turns out that these clusters are hypoelectronic,[20] with fewer valence electrons than generally observed for a canonical *arachno*-structure of the same nuclearity.

The average B−B distances of clusters **3** and **4**, (**3**: 1.75, **4**: 1.76 Å) are comparable with **2** and other tantalaborane clusters;[10,21] however, the average Ta−B (2.38 Å) and Ta−Ta (3.23 Å) distances are about 0.1 and 0.3 Å longer than observed

dx.doi.org/10.1021/ic300848f | Inorg. Chem. 2012, 51, 10176−10184

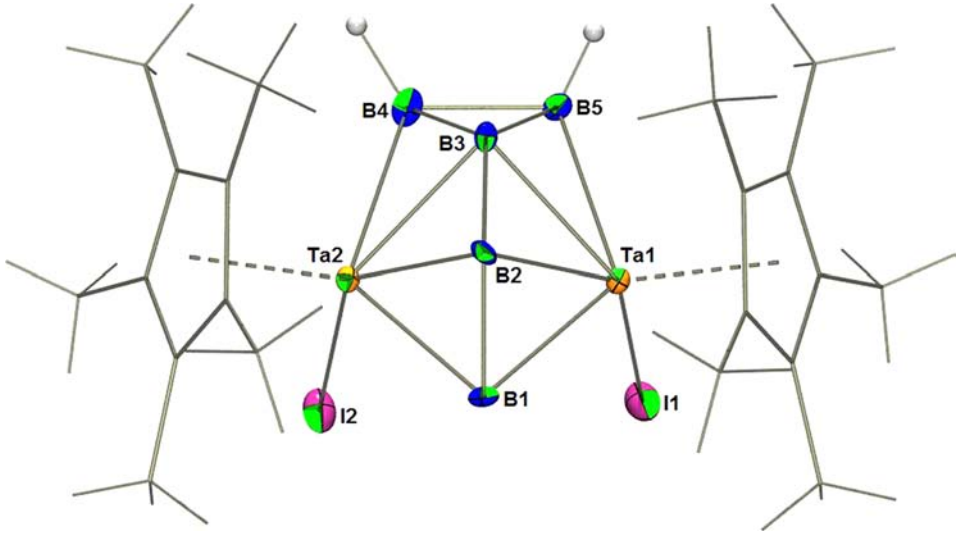

Figure 2. Molecular structure for $[(Cp^*TaI)_2B_5H_{11}]$ **4**. Selected bond lengths (Å) and angles (deg): Ta1−Ta2 3.2376(4), Ta1−I1 2.8185(5), Ta2−I2 2.8492(5), Ta1−B2 2.275(7), Ta1−B3 2.416(7), Ta1−B1 2.417(8), Ta1−B5 2.434(7), Ta2−B2 2.249(8), Ta2−B1 2.413(7), Ta2−B3 2.437(8), Ta2−B4 2.421(8), B1−B2 1.755(10), B2−B3 1.723(10), B3−B5 1.752(9), B3−B4 1.786(10), B4−B5 1.827(11); B2−Ta1−B1 43.8(3), B(2)−Ta(1)−Ta(2) 43.98(19), B1−Ta1−Ta2 47.86(18), B5−Ta1−Ta2 72.98(18).

Table 1. DFT Calculated[a] and Experimental NMR Chemical Shifts δ (ppm) for the Clusters $[(Cp^*TaCl)_2B_5H_{11}]$ (2), $[(Cp^*TaBr)_2B_5H_{11}]$ (3), $[(Cp^*TaI)_2B_5H_{11}]$ (4), and $[(Cp^*TaF)_2B_5H_{11}]$ (7)

	BP86 [B3LYP] (Exp.)				BP86 [B3LYP]
cluster δ	**1**[9]	**2**[9]	**3**	**4**	**7**
			^{11}B NMR		
B1	9.0 [13.1] (23.9)	0.9 [10.0] (15.1)	7.0 [14.1] (22.4)	13.1 [20.8] (24.7)	−7.6 [−0.4]
B2	−12.2 [−6.2] (3.7)	58.6 [72.0] (77.7)	60.3 [74.4] (81.1)	62.5 [76.4] (78.9)	52.3 [64.9]
B3	27.7 [36.2] (44.8)	−21.2 [−14.4] (−10.0)	−21.1 [−14.2] (−8.3)	−21.6 [−15.2] (−11.9)	−20.8 [−14.9]
B4	−12.1 [−5.9] (3.7)	7.5 [12.5] (18.8)	9.9 [14.9] (23.8)	13.3 [18.7] (25.8)	1.5 [6.6]
B5	8.8 [13.1] (23.9)	7.5 [12.2] (18.8)	9.9 [14.5] (23.8)	13.4 [18.0] (25.8)	1.5 [5.7]
			^{1}H NMR		
H6	2.61 [2.54] (5.43)	1.73 [1.98] (2.91)	1.91 [2.17] (3.28)	2.14 [2.41] (2.32)	1.63 [1.83]
H7	0.89 [0.9] (4.39)	4.77 [4.98] (3.80)	4.90 [5.1] (4.10)	5.12 [5.35] (4.08)	4.34 [4.26]
H8	0.82 [1.11] (3.14)	−0.34 [−0.35] (2.82)	−0.37 [−0.37] (3.05)	−0.41 [−0.46] (2.04)	−0.25 [−0.38]
H9	0.9 [0.81] (4.39)	2.29 [2.35] (4.18)	2.43 [2.46] (4.52)	2.58 [2.69] (4.32)	2.14 [2.25]
H10	2.58 [2.54] (5.43)	2.30 [2.20] (4.18)	2.43 [2.30] (4.52)	2.58 [2.52] (4.32)	2.14 [2.03]
H11	−4.73 [−4.4] (−3.93)	−3.67 [−3.84] (−2.76)	−3.49 [−3.71] (−2.94)	−3.50 [−3.87] (−3.72)	−3.27 [−3.42]
H12	−9.15 [−8.96] (−6.65)	−3.67 [−4.01] (−2.76)	−3.50 [−3.86] (−2.94)	−3.50 [−3.90] (−3.72)	−3.26 [−3.63]
H13	−9.87 [−10.49](−6.65)	−3.63 [−3.79] (−2.38)	−3.46 [−3.69] (−2.45)	−3.45 [−3.71] (−3.64)	−3.61 [−3.61]
H14	−9.84 [−10.22](−6.65)	−3.61 [−3.86] (−2.38)	−3.45 [−3.75] (−2.45)	−3.44 [−3.81] (−3.64)	−3.59 [−3.82]
H15	−9.13 [−9.05](−6.65)	0.08 [0.16] (−0.06)	0.25 [0.35] (−0.12)	0.44 [0.50] (−0.14)	0.10 [0.21]
H16	−4.85 [−4.44] (−3.93)	2.91 [3.70] (8.58)	3.21 [3.96] (7.82)	2.68 [3.42] (7.86)	2.96 [3.60]
H_{Cp^*}	1.70 [1.9] (2.16)	1.96 [2.17] (1.87)	2.01 [2.27] (2.12)	2.03 [2.19] (2.18)	2.13 [2.25]
			^{13}C NMR		
C51	115.92 [120.78] (110.80)	112.33 [116.32] (116.80)	111.91 [116.25] (116.80)	111.53 [115.41] (116.20)	114.01 [118.23]
C56	10.03 [9.74] (12.90)	8.75 [8.08] (14.40)	8.81 [8.16] (12.80)	8.86 [8.16] (13.60)	8.58 [8.08]

[a]BP86/TZ2P and B3LYP/TZ2P all-electron basis set.

in the parent molecule **1**. The Ta−Ta distance is too long for a full Ta−Ta single bond (cf. 2.9261 in the parent molecule **1**[9] or 2.854 Å in $[(\eta^5\text{-}C_5Me_4EtTa)_2Cl_3H_2(Me)]$[22]); however, it is too short to propose that there is no interaction at all between the two metal centers.[23] Another interesting feature of **2**−**4** is the presence of a bridging hydride ligand between the two metal centers. Usually, a bridging hydride ligand pull the metals together to form a three-center-two-electron bonding system;[24] however, this is in marked contrast to **2**−**4** where the M-M distances are too large for a significant binding interaction (**2**: 3.2219, **3**: 3.2280, **4**: 3.2376 Å). Although all of the BH terminal protons and bridging protons were not located in the X-ray diffraction study, evidence for their presence has been supported by the $^1H\{^{11}B\}$ NMR spectrum as well as DFT calculations (vide infra).

Electronic Structure Analysis. Geometry of the clusters **2**−**4** and the hypothetical cluster $[(Cp^*TaF)_2B_5H_{11}]$ (**7**) were first optimized and compared. The selected calculated bond lengths and bond angles are listed in the Supporting Information, Table S1 (see Supporting Information, Scheme

dx.doi.org/10.1021/ic300848f | *Inorg. Chem.* 2012, 51, 10176−10184

S1 for the atom numbering). Satisfactory agreement is observed between computed bond lengths and those of the crystallographically characterized clusters **2**−**4**. Interestingly, the B−B distances are slightly shorter than the parent molecule **1** (Supporting Information, Table S1). Computed B−H and Ta−H bond parameters of these hydrogens are also listed in Supporting Information, Table S1. They are in good agreement with the values reported previously in related clusters. We also checked the presence of the hydride ligand (H16) that bridges the two metal centers. Replacing this hydride by a negative charge in clusters **2**−**4** and **7** resulted in lengthening of the Ta−Ta bond length of about 0.25 Å (3.451 Å in **2**, 3.473 Å in **3**, 3.504 Å in **4**, and 3.378 Å in **7**). Thus the bridging hydrogen atom plays an important role for keeping the two Ta atoms close to each other.

The experimentally measured ^{1}H and ^{11}B NMR spectra, given in Table 1, are consistent with the solid state X-ray structure of **3** and **4**. The chemical shifts at δ 23.8 and 22.4 ppm (for **3**) and 25.8 and 24.7 ppm (for **4**) can be assigned to the pair of equivalent boron atoms B4 and B5 and unique boron B1, respectively (Figure 1 and 2). The other two resonances of intensity one can be assigned to the unique four- and five-connect boron atoms B2 and B3, respectively. The two pairs of equivalent Ta−H−B and one B−H−B hydrogen can be placed as shown in Scheme 1. In the ^{1}H NMR spectrum of **3** and **4**, a hydride resonance of area one relative to the Cp* group (η^5-C_5Me_5 = 30H) are found at δ 7.82 and 7.86 ppm respectively. A good agreement is observed for the ^{11}B chemical shift values (maximum deviations of 0−10 ppm with B3LYP/TZ2P level and 0−20 ppm with BP86/TZ2P level) in the upfield region as similar to those computed for other metallaboranes.[14,25] In clusters **2**, **3**, **4**, and **7** the three-connect boron atoms B1 (2Ta, 1B) and B4, B5 (1Ta, 2B) theoretically show resonances at rather high field in the range from 15 to −10 ppm, with the latter slightly more deshielded. The four-connect boron atom B2 (2Ta, 2B) resonates at very low field at about 60 ppm. Finally, the five-connect boron atom B3 (2Ta, 3B) is highly shielded at about −20 ppm. As shown in Table 1, a very good agreement is also observed for the ^{1}H chemical shifts, confirming the proposed location of the bridging protons. They all resonate in the −4 to +5 ppm region. The resonances for terminal hydrogens (H6−10) are slightly more upfield (ca.3 to 5 ppm) than those computed for the Ta−H−B bridging hydrogens (ca. −3 to −4 ppm for H11−14).

Although, the pathway for the formation of **2**−**4** from **1** is of interest, we were unable to obtain any direct information. However, note that products **2**−**4** can arise from the addition of halogens (X = Cl, Br, I) to the Ta−Ta bond in **1**. In accord with this interpretation, the tantalum−tantalum distance lengthens from 2.926 Å in **1** to 3.222−3.237 Å in **2**−**4**. The six bridging hydrogen atoms in **1** reorganize in **2**−**4** so that one of the six hydrogen atoms bridges the Ta−Ta bond. Furthermore, in comparison with **1**, the tantalum atoms in **2**−**4** are far away from each other, which in turn lead to a rearrangement of the five boron atoms. Thus in **1**, the five boron atoms form a chain. However, in **2**−**4** three of the five boron atoms form a B_3 triangle and the remaining two boron atoms are attached to one of the vertices of the B_3 triangle as a chain.

The highest occupied molecular orbital (HOMO) and the lowest unoccupied molecular orbital (LUMO) energies as well as the HOMO−LUMO gap for the clusters **2**−**4** and **7** are listed in Supporting Information, Table S1. The computed substantial HOMO−LUMO gap of **2**−**4** and **7** is around 2 eV, which indicates the viability of these clusters.[26] Nevertheless, it is slightly smaller than that computed for the parent cluster **1** which is 2.3 eV. As expected with respect to the electronegativity of the halogens, this HOMO−LUMO gap decreases going from F to I (2.1 (**7**), 2.0 (**2**), 1.9 (**3**), and 1.7 (**4**) eV). A more realistic indicator of geometric stability is ionization potential (IP) energy. The first vertical and adiabatic IPs for one-electron loss were computed for **1**−**4** and **7** (Figure 3). A

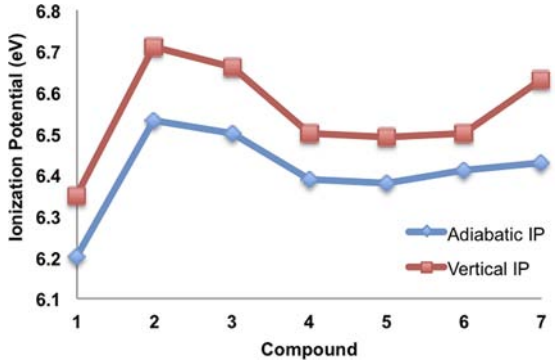

Figure 3. First vertical and adiabatic ionization potentials (eV) for clusters **1**−**7**.

large value above 6 eV indicates the stable nature of these clusters. The vertical curve is a few tenths of an eV higher in energy as expected, because of a significant geometry change upon ionization.

Using the classical PSEPT electron counting formalism,[19] the parent molecule $[(Cp^*Ta)_2B_5H_{11}]$ **1**, can be viewed as an electron-deficient *oblatonido* species with its structure derived from an 8-vertex *oblatocloso* hexagonal bipyramidal cluster encountered for the *apparent* 6-sep cluster $[(Cp^*Re)_2B_6H_4Cl_2]$.[14] The cluster **1** has the same sep count of 6 ([−2 (Cp*Ta) × 2 + 2 (BH) × 5 + 1 (bridging H) × 6]/2), and shows a somewhat short metal−metal cross-cluster bond. In the same way, clusters **2**−**4** and **7** are 7-vertex *oblatoarachno* M_2B_5 clusters with 7 sep. This electron count is obtained considering that the ML_4 fragments Cp*TaX are −1 electron entities with 3 frontier orbitals rather than −3 electron moieties with two frontier orbitals, according to an extended Hückel fragment analysis performed on **2**. With a count of 7 sep, clusters **2**−**4** and **7** possess one sep more than the parent species **1**. This could explain why the metal−metal cross-cluster bond length is considerably shorter in **1** (2.94 Å in **1** vs. over 3.20 Å in **2**−**4** and **7**).

Further insight in the nature of the bonding between the Ta atoms in clusters **2**−**4** can be provided by an analysis of the electron localization function (ELF).[27] Being directly related to the electron pair probability density, its graphical representation can contribute to the understanding of electron localization and therefore the degree of metal−metal interaction. The ELF values vary from 0 to 1, the upper limit corresponding to perfect electron-pair localization, that is, important covalent character, whereas the reference value of 0.5 corresponds to a perfect delocalization (homogeneous electron gas).

Two-dimensional electron density distribution plots in planes containing the two Ta atoms are sketched in Figure 5 for **2** and its parent cluster **1**. The two plots show rather high delocalization domains between the metal atoms. It has been shown that this is generally the case for complexes with M-M

dx.doi.org/10.1021/ic300848f | *Inorg. Chem.* 2012, 51, 10176−10184

interactions.[28] Nevertheless, delocalization (i.e., smaller values of ELF) is much more important for cluster **2** which exhibits a rather long Ta−Ta distance of 3.222 Å. This suggests a weak Ta−Ta interaction only. For comparison, the ELF plot for the known $[Ta_2(PMe_3)_4Cl_4(\mu\text{-}H)_2]$ **8**,[29] shown in Figure 4, shows a

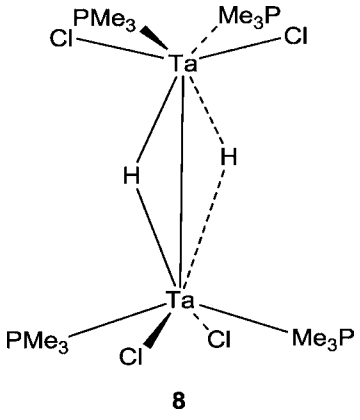

8

Figure 4. Structure of $[Ta_2(PMe_3)_4Cl_4(\mu\text{-}H)_2]$ (**8**).

very short Ta−Ta separation of 2.545 Å associated to a double bond character, which indicates a weaker delocalization with an ELF value of about 0.6 (see bottom of Figure 5).

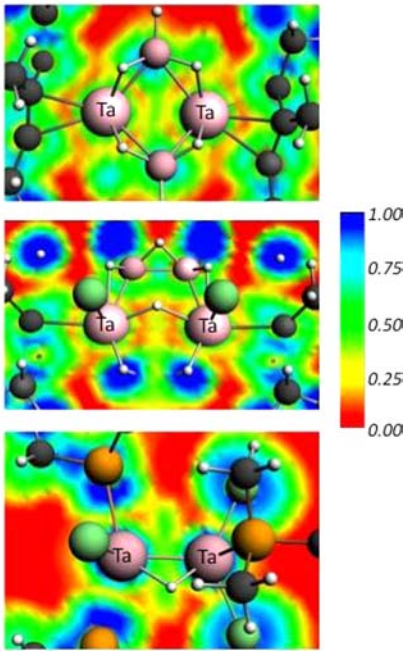

Figure 5. ELF plots (DFT) for clusters **1** (in the Ta−C(Cp)-Ta plane), top), **2** (in the Ta−B4−Ta plane, middle), and **8** (in the Ta−Cl−Ta plane, bottom).

The weak Ta−Ta interaction in **2** (and probably in its congeners **3**, **4**, and **7**) is supported by the DFT calculated bond multiplicity (BM) indices based on the Nalewajski−Mrozek method.[30] This approach incorporates both covalent and ionic contributions to valency and yields BM indices, analogous to bond orders, that generally correlate well with the experimental interatomic distances as well as chemically intuitive descriptions of bonding.[31] Indeed, the Ta−Ta bond index in clusters **2**−**4** and **7** is 0.23 weaker than the corresponding value in **1**, which is 0.58. These values agree well with the experimentally observed and computed Ta−Ta distances, and indicate the delocalized nature in these clusters—values far from 1 are found even for **1**—and poor metal−metal interaction in clusters **2**−**4** and **7**. For comparison, the Ta−Ta bond index calculated for **8** is 1.80 which strongly agrees with the presence of double bond between the metal atoms in this cluster. In all the clusters studied, the computed Ta−C bond multiplicities are in the range of 0.23 to 0.38, whereas the Ta−B ones are in the range of 0.30 to 0.67 (see Supporting Information, Table S2).

Since there are no experimental thermodynamic data available for clusters **2**−**4** and **7**, we tried to gain some insight about their stability by computing their enthalpies of reaction (ΔH_r at 0 K = difference in bond energies of the product and the reactants) assuming eq 1: The computed ΔH_r values, −7.24 eV for **7** (X = F), −3.67 eV for **2** (X = Cl), −3.05 eV for **3** (X = Br), and −2.05 eV for **4** (X = I), indicate highly exothermic reactions, that is, high thermodynamic stability. For comparison, the hypothetical isomer of **2** with the core geometry of **1**, **1-Cl$_2$** (Figure 6), is computed to be 2.36 eV less stable than **2**.

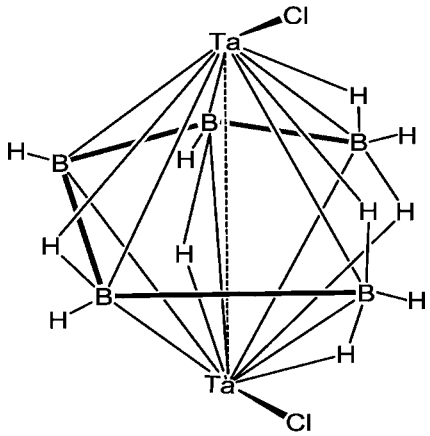

1-Cl$_2$

Figure 6. Hypothetical cluster **1-Cl$_2$**.

Evidently, the addition of X_2 (i.e., the addition of two electrons) to cluster **1** leads to a substantial rearrangement of the Ta_2B_5 cage with some metal−metal elongation and formation of a new B−B bond.

$$[(Cp^*Ta)_2B_5H_{11}] + X_2 \rightarrow [(Cp^*TaX)_2B_5H_{11}]$$
$$X = F, Cl, Br, \text{or } I \qquad (1)$$

Reactivity of 5 with I$_2$. The metallaborane clusters, in general, offer reaction possibilities similar to that of polyhedral boranes and transition metal clusters, however, with the added feature of competition between metal and boron sites, for example, borane displacement vs metal fragment displacement, ligand substitution at boron vs metal sites, removal of M-H-M vs M−H-B vs B−H−B protons, and so forth.[4,5,32] As cluster **5** bears similar structural and formula relationship to $[(Cp^*Ta)_2B_5H_{11}]$, we performed the reaction of **5** in the presence of I_2, and the attack at a boron site was evidenced by the formation of **6** (Scheme 2). Cluster **6** has been isolated in good yield and characterized spectroscopically as well as by single crystal X-ray diffraction analysis. The molecular ion peak in the FAB mass spectrum corresponds to $[(Cp^*Ta)_2B_5H_{12}I]$.

dx.doi.org/10.1021/ic300848f | Inorg. Chem. 2012, 51, 10176−10184

Scheme 2. Synthesis of Tantalaborane Derivative 6

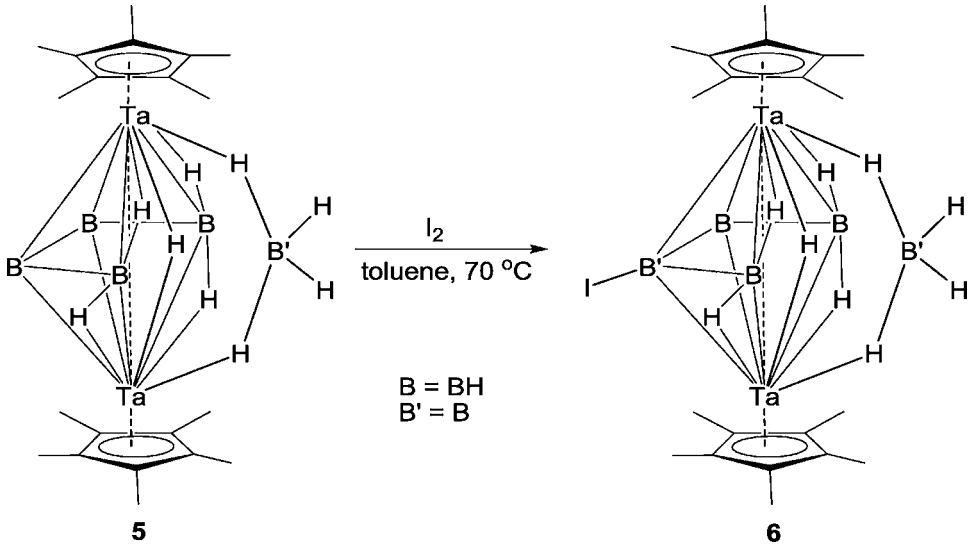

The IR spectrum of **6** features bands at 2462 and 2384 cm^{-1} due to the terminal B−H stretches. The ^{11}B NMR spectrum of **6** exhibits five signals at δ 21.5, 18.1, 13.9, −1.5, and −19.9 ppm with equal intensity ratio. The chemical shift at δ 21.5 ppm is ascribed to the B−I as it remained singlet in coupled ^{11}B NMR spectrum. The $^{1}H\{^{11}B\}$ spectrum of **6** suggests the presence of three kinds of terminal hydrogen atoms at δ 5.5, 4.7, and 4.1 ppm (1:1:1) and two kinds of bridging hydrogen atoms. In addition, one broad quartet appearing as almost flat humps centered at δ −10.3 ppm, which can be assigned to BH_4^- protons. This is consistent with a fluxional behavior of the coordinated BH_4^- ion in solution and exactly similar to that observed for **5**.

The ^{11}B and ^{1}H NMR chemical shift values computed for clusters **5** and **6** are given in Table 2 (see Supporting Information, Scheme S2 for the atom numbering). They are in a rather good agreement with the experimental values. A deviation of about 0−10 ppm, at both B3LYP/TZ2P and BP86 levels, is observed for the ^{11}B chemical shifts values within the trend measured experimentally. The deviation of more than 20 ppm observed for B5 in **5** and **6**, is attributed to the observed fluxional nature of B5 in solution whereas the computed values are in gas phase. The four-connect boron atoms B2 and B3 resonate at about 15 ppm in **5**. In cluster **6**, B2 is more deshielded and resonates at a lower field at δ 29.4 ppm because of the substitution of the terminal hydrogen by iodine for hydrogen, whereas B3 resonates around 12 ppm. In accord with the measured ^{11}B NMR chemical shifts, the computed values for B1 and B4 in cluster **5** are similar (δ 2.2 and 1.8 ppm, respectively). The computed ^{1}H NMR values (Table 2) are also in good agreement with the experimental values with a maximum deviation of 2 ppm, except for H10 and H11 which are terminal hydrogens of the BH_4^- ion (difference of 11 ppm). The satisfactory agreement has been observed for B−H_t terminal, the Ta−H−B bridging and the Ta−H−Ta bridging hydrogen atoms.

A solid-state structure determination of **6**, shown in Figure 7, shows one tetrahydroborate ligand coordinated to the unit $[(Cp^*Ta)_2B_4H_8I]$, via two Ta−H−B bridge bonds. The B−I distance (2.199(19) Å) is longer comparable to that observed in BI_3.[33] All the bridging and terminal hydrogen atoms have not been positioned by X-ray diffraction studies, however their connectivity have been assertively determined by low temperature $^{1}H\{^{11}B\}$ NMR. The geometries of **5** and **6** were theoretically optimized. The DFT computed bond parameters in general are in good agreement with the experimental values (see Supporting Information, Table S3).

Table 2. DFT Calculated[a] and Experimental NMR Chemical Shifts δ (ppm) for the Clusters $[(Cp^*Ta)_2B_5H_{13}]$ (5) and $[(Cp^*Ta)_2B_5H_{12}I]$ (6)

	BP86 [B3LYP] (Exp.)	
δ	**5**[10]	**6**
	^{11}B NMR	
B1	2.2 [9.1] (−0.1)	2.4 [8.6] (13.9)
B2	15.1 [26.0] (15.7)	29.3 [37.6] (21.4)
B3	14.4 [25.2] (15.7)	11.7 [21.7] (18.1)
B4	1.8 [8.6] (−0.1)	2.5 [9.8] (−1.4)
B5	−46.2 [−43.1] (−20.8)	−46.2 [−42.9] (−19.9)
	^{1}H NMR	
H6	2.75 [2.82] (5.95)	3.31 [3.37] (5.56)
H7	1.99 [2.32] (2.29)	
H8	1.94 [2.27] (2.29)	2.33 [2.65] (4.19)
H9	2.80 [2.85] (5.95)	2.76 [2.87] (4.71)
H10	−0.06 [0.39] (−10.91)	−0.14 [0.32] (−10.34)
H11	−0.02 [0.41] (−10.91)	−0.33 [0.12] (−10.34)
H12	−8.44 [−8.36] (−7.40)	−7.72 [−7.62] (−6.87)
H13	−8.42 [−8.35] (−7.40)	−7.71 [−7.66] (−6.87)
H14	−8.17 [−8.08] (−7.40)	−8.44 [−8.47] (−6.91)
H15	−8.12 [−8.04] (−7.40)	−8.46 [−8.48] (−6.91)
H16	−3.17 [−2.65] (−10.91)	−3.79 [−3.37] (−10.34)
H17	−3.21 [−2.7] (−10.91)	−3.79 [−3.39] (−10.34)
H18	−7.60 [−6.13] (−10.91)	−8.32 [−7.12] (−10.34)
H_{Cp^*}	1.65 [1.59] (2.16)	3.01 [2.93] (2.33)
	^{13}C NMR	
C51	111.36 [115.29] (109.30)	110.83 [115.05] (117.3)
C56	8.40 [8.28] (12.84)	7.12 [7.87] (13.15)

[a]BP86/TZ2P and B3LYP/TZ2P all-electron basis set.

Within the classical PSEPT electron counting formalism,[19] clusters **5** and **6** can be considered as electron-deficient *oblatoarachno* Ta_2B_4 species with their structure derived from an 8-vertex *oblatocloso* hexagonal bipyramidal, encountered for $[(Cp^*Re)_2B_6H_4Cl_2]$,[14] by removal of two adjacent BH units in

dx.doi.org/10.1021/ic300848f | Inorg. Chem. 2012, 51, 10176−10184

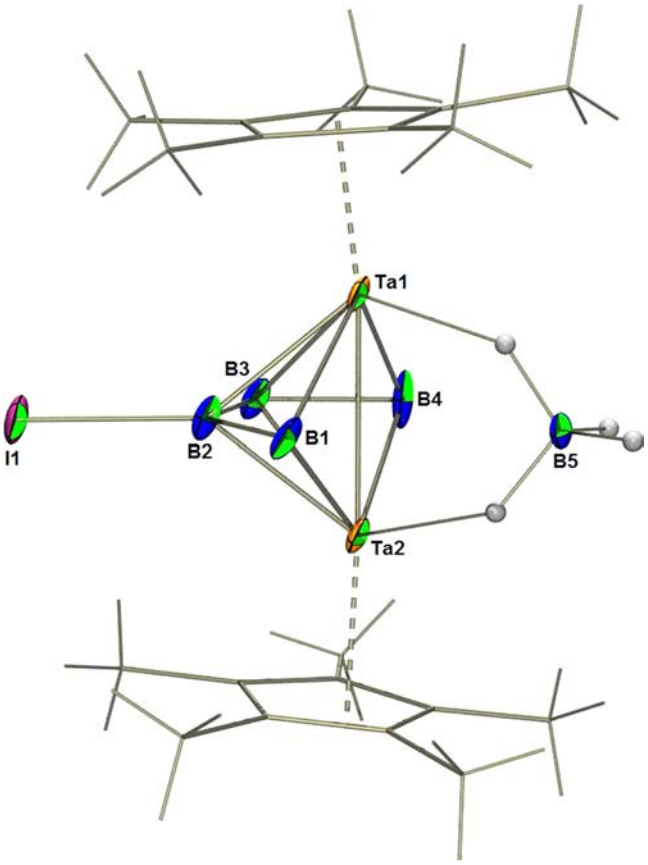

Figure 7. Molecular structure and labeling diagram of **6**. Selected bond lengths (Å) and angles (deg): Ta1−Ta2 2.8773(10), B1−B2 1.76(3), B2−B3 1.74(3), B3−B4 1.83(3), Ta1−B1 2.39(2), Ta2−B1 2.40(2), Ta1−B2 2.29(2), Ta2−B2 2.284(19), Ta1−B3 2.37(2), Ta2−B3 2.339(19), Ta1−B4 2.47(2), Ta2−B4 2.36(2), B2−I1 2.199(19); Ta1−B1−Ta2 73.8(6), Ta1−B2−Ta2 78.0(6), Ta1−B3−Ta2 75.4(6), Ta1−B4−Ta2 73.1(7).

the hexagon. The BH_4^- anion should be considered as a 4-electron donor ligand weakly bound in a bidentate coordination mode[34] to the cluster leading to reformulate species **5** and **6** as $[(Cp^*Ta)_2B_4H_9]^+(\mu\text{-}BH_4^-)$ and $[(Cp^*Ta)_2B_4H_8I]^+(\mu\text{-}BH_4^-)$ respectively. In accord with polyhedral electron pair theory,[19] this geometry should be associated with 6 sep ([−2 (Cp*Ta) × 2 + 2 (BH/BI) × 4 + 1 (bridging H) × 5 + 4 (BH_4^-) × 1 − 1 (charge)]/2). This is the same count as those observed in the *oblatocloso* cluster $[(Cp^*Re)_2B_6H_4Cl_2]$ and **1**. The HOMO−LUMO energy gaps of 2.4 and 2.2 eV, for **5** and **6** respectively, are indicative of high stability. Similarly, the vertical and adiabatic IPs of 6.5 and 6.4 eV for **5** and **6**, respectively, are comparable to those of **1**−**4** and **7** (see Figure 3). The calculated Ta−Ta BM indices for **5** and **6** are 0.39 and 0.41, respectively, rather weaker than in **1** (0.58).

CONCLUSION

The present study provides an insight into the formation of open cage *oblatoarachno* tantalaboranes **2**−**4**, from the reaction of *nido*-tantalaborane, **1**, with different halogen sources. The clusters **2**−**4** and **7** can be viewed as 7-sep 7-vertex *oblatoarachno* M_2B_5 clusters, which can be generated from a 7-sep 9-vertex *oblatocloso* M_2B_7 cluster by removal of two equatorial boron atoms. On the other hand, cluster **6** can be considered as an electron-deficient 6-sep 6-vertex *oblatoarachno* M_2B_4 cluster derived from an 8-vertex *oblatocloso* hexagonal bipyramidal cluster, and BH_4^- anion weakly bonded in a bidentate mode. The experimental results were complemented and rationalized by means of DFT studies that reveal that geometries are in agreement with the structure determinations. The large HOMO−LUMO differences and the enthalpies of reaction calculated are in good accord with their stabilities.

EXPERIMENTAL SECTION

General Procedures and Instrumentation. All the operations were conducted under an Ar/N_2 atmosphere using standard Schlenk techniques. Solvent were distilled prior to use under Argon. $[Cp^*TaCl_4]$, $[BH_3{\cdot}thf]$, and $[LiBH_4{\cdot}thf]$ were used as received (Aldrich). The $[(Cp^*Ta)_2B_5H_{11}]$[9] and $[(Cp^*Ta)_2B_4H_9(\mu\text{-}BH_4)]$[10] were synthesized according to the literature method. The external reference $[Bu_4N(B_3H_8)]$, for the ^{11}B NMR was synthesized with the literature method.[35] Preparative thin-layer chromatography was performed with Merck 105554 TLC Silica gel 60 F_{254}, layer thickness 250 μm on aluminum sheets (20 × 20 cm). NMR spectra were recorded on a 400 and 500 MHz Bruker FT-NMR spectrometer. Residual solvent protons were used as reference (δ, ppm, C_6D_6, 7.15), while a sealed tube containing $[Bu_4N(B_3H_8)]$ in C_6D_6 (δ_B, ppm, −30.07) was used as an external reference for the ^{11}B NMR. Infrared spectra were recorded on a Thermo Nicolet iS10 FT spectrometer. Mass spectra were obtained on a Jeol SX 102/Da-600 mass spectrometer with argon/xenon (6kv, 10 mÅ) as FAB gas.

General Procedure for Synthesis of $[(Cp^*TaX)_2B_5H_{11}]$ (X = Cl, Br, I), 2−4. To a flame-dried Schlenk tube containing 0.05 g of $[(Cp^*Ta)_2B_5H_{11}]$ (0.07 mmol) in toluene (10 cm^3), excess of CH_2Br_2 was added via syringe, and the reaction mixture was thermolyzed at 60 °C for 20 h. The solvent was evaporated under vacuum; the residue was extracted into hexane and passed through Celite. The mother liquor was concentrated and chromatographed on a silica gel TLC plates. Elution with a hexane/CH_2Cl_2 (70:30 *v*/*v*) mixture yielded the red band **3** (0.051 g, 83%). Under the same reaction conditions **2** (0.048 g, 87%) and **4** (0.053 g, 77%), were isolated from the reaction of $[(Cp^*Ta)_2B_5H_{11}]$ with CH_2Cl_2 and I_2 respectively. Further, in a similar fashion, reaction of **5** (0.06 g, 0.09 mmol) with I_2 (0.07 g, 0.27 mmol) yielded **6** (0.04 g, 56%).

Reaction of $[(Cp^*Ta)_2B_5H_{11}]$, **1**, with a fluorinating agent, KF, was examined; however, incorporation of fluorine atom into cluster **1** failed, under the same reaction conditions.

3: ^{11}B NMR (128 MHz, C_6D_6, 22 °C): δ 81.1 (s, 1B), 23.8 (s, 2B), 22.4 (s, 1B), −8.3 ppm (s, 1B). ^1H NMR (400 MHz, C_6D_6, 22 °C): δ 7.82 (s, 1Ta−H−Ta), 4.52 (partially collapsed quartet (pcq), $2BH_t$), 4.10 (pcq, $1BH_t$), 3.28 (pcq, $1BH_t$), 3.05 (pcq, $1BH_t$), 2.12 (s, 30H; Cp*), −0.12 (br, 1B−H−B), −2.45 (br, 2Ta−H−B), −2.94 ppm (br, 2 Ta−H−B). ^{13}C NMR (100 MHz, C_6D_6, 22 °C): δ 116.8 (s; C_5Me_5), 12.8 (s; CH_3 in C_5Me_5). IR (hexane): 2441w, 2490w (BH_t). MS (FAB) P^+(max): 857; Elemental analysis calcd (%) for $C_{26}H_{31}B_1Fe_1Ta_2O_6$: C, 28.01; H, 4.82. Found: C, 28.35; H, 4.81.

4: ^{11}B NMR (128 MHz, C_6D_6, 22 °C): δ 78.9 (s, 1B), 25.8 (s, 2B), 24.7 (s, 1B), −11.9 ppm (s, 1B). ^1H NMR (400 MHz, C_6D_6, 22 °C): δ 7.86 (s, 1Ta−H−Ta), 4.32 (pcq, $2BH_t$), 4.08 (pcq, $1BH_t$), 2.32 (pcq, $1BH_t$), 2.04 (pcq, $1BH_t$), 2.18 (s, 30H; Cp*), −0.14 (br, 1B−H−B), −3.64 (br, 2Ta−H−B), −3.72 ppm (br, 2 Ta−H−B). ^{13}C NMR (100 MHz, C_6D_6, 22 °C): δ 116.2 (s; C_5Me_5), 13.6 (s; CH_3 in C_5Me_5). IR (hexane): 2451w, 2482w (BH_t). MS (FAB) P^+(max): 951. Elemental analysis calcd (%) for $C_{26}H_{31}B_1Fe_1Ta_2O_6$: C, 25.25; H, 4.34. Found: C 25.02, H 4.51.

6: ^{11}B NMR (128 MHz, C_6D_6, 22 °C): δ 21.4 (s, 1B), 18.1 (d, 1B; BH), 13.9 (d, 1B; BH), −1.4 (d, 1B; BH), −19.9 (br, 1B; BH_4). ^1H NMR (400 MHz, C_6D_6, 22 °C): δ 5.56 (pcq, $1BH_t$), 4.71 (pcq, $1BH_t$), 4.19 (pcq, $1BH_t$), 2.33 (s, 30H, 2Cp*), −6.87 ppm (pcq, 2Ta−H−B), −6.91 ppm (pcq, 2Ta−H−B), −10.34 (br, 4H, BH_4). ^{13}C NMR (100 MHz, C_6D_6, 22 °C): δ 117.3 (s; C_5Me_5), 13.15 (s; C_5Me_5). IR (hexane): 2462 and 2384 (BH_t). MS (FAB) P^+(max): 825. Elemental analysis calcd (%) for $C_{26}H_{31}B_1Fe_1Ta_2O_6$: C, 29.10; H, 5.12. Found: C, 28.92; H, 4.95.

dx.doi.org/10.1021/ic300848f | *Inorg. Chem.* 2012, 51, 10176−10184

X-ray Structure Determination. Crystal data for **3** and **6** were collected and integrated using a Bruker AXS kappa apex2 CCD diffractometer, with graphite monochromated Mo−Kα (λ = 0.71073 Å) radiation at 293 K. Crystal data for **4** were collected and integrated using an Oxford Diffraction Xcalibur-S CCD system equipped with graphite-monochromated Mo Kα radiation (λ = 0.71073 Å) radiation at 150 K. The structures were solved by heavy atom methods using SHELXS-97 or SIR92[36] and refined using SHELXL-97 (Sheldrick, G.M., University of Göttingen).[37]

Crystal data for **3**: CCDC 871795, Formula $C_{20}H_{39}B_5Br_2Ta_2$, Crystal system, space group: monoclinic, $P2_1/n$, a = 8.0765(3), b = 15.3522(5), c = 21.2837(7)Å, β = 97.937(2)°, Z = 4, ρ_{calcd} = 2.173 Mg/m^3, Final R indices [$I > 2\sigma(I)$] R_1 = 0.0405, wR^2 = 0.0717, Index ranges $-8 \le h \le 10$, $-21 \le k \le 21$, $-29 \le l \le 18$, Crystal size 0.15 × 0.15 × 0.09 mm^3, Reflections collected 21499, independent reflections 6811, [R(int) = 0.0496], Goodness-of-fit on F^2 1.044.

Crystal data for **4**: CCDC 871796, Formula $C_{40}H_{64}B_{10}I_4Ta_4$, Crystal system, space group: Monoclinic, $P2_1/n$, a = 16.0832(2), b = 15.5579(2),c = 22.0241(3) Å, β = 103.4050(10)°, Z = 4, ρ_{calcd} = 2.335 Mg/m^3, Final R indices [$I > 2\sigma(I)$] R1 = 0.0259, wR2 = 0.0531, Index ranges $-19 \le h \le 18$, $-18 \le k \le 18$, $-26 \le l \le 25$, Crystal size 0.36 × 0.33 × 0.28 mm^3, Reflections collected 39696, independent reflections 9427, [R(int) = 0.0393], Goodness-of-fit on F^2 0.941.

Crystal data for **6**: CCDC 871794, Formula $C_{20}H_{34}B_5ITa_2$, Crystal system, space group: Monoclinic, $P2_1/c$, a = 18.456(3), b = 13.8228(19), c = 10.2642(14) Å, β = 92.579(7)°, Z = 4, ρ_{calcd} = 2.075 Mg/m^3, Final R indices [$I > 2\sigma(I)$] R1 = 0.0723, wR2 = 0.1862, Index ranges $-21 \le h \le 21$, $-14 \le k \le 16$, $-12 \le l \le 12$, Crystal size 0.20 × 0.18 × 0.15 mm^3, Reflections collected 15055, independent reflections 4601, [R(int) = 0.0757], Goodness-of-fit on F^2 1.058.

Computational Details. DFT calculations were carried out using the Amsterdam Density Functional (ADF) program[38] developed by Baerends and co-workers.[39] The Vosko−Wilk−Nusair parametrization[40] was used for the local density approximation (LDA) with gradient corrections for exchange (B88)[41] and correlation (P86) (BP86 functional).[42] The geometry optimization procedure was based on the method developed by Versluis and Ziegler.[43] Relativistic corrections were added using the ZORA (zeroth order regular approximation) scalar Hamiltonian.[44] Structures are initially optimized using TZP basis set which is available in the ADF program, by taking experimental geometries as inputs. Further, the BP86/TZP optimized geometries are used as inputs for the optimization and NMR computations using all-electron TZ2P basis set[38,39] at relativistic scalar ZORA level of calculations. NMR chemical shifts were also calculated with the hybrid Becke−Lee−Yang−Parr (B3LYP) functional[45] by using the BP86/TZ2P optimized geometries. The B3LYP method has been found to be somewhat more reliable than the BP86 one for this type of calculations. Both are given for comparison.[46] Computation of the NMR shielding tensors employed gauge-including atomic orbitals (GIAOs),[47] using the implementation of Schreckenbach, Wolff, Ziegler, and co-workers.[48,49] TMS ($SiMe_4$) was used as an internal standard for the ^{1}H NMR. The projected ^{11}B chemical shielding values, determined from relativistic scalar ZORA calculations were referenced to B_2H_6 as the primary reference point, and these chemical shift values (δ) were then converted to the standard $BF_3{\cdot}OEt_2$ scale using the experimental value of +16.6 ppm for B_2H_6. The fragment analysis of **2** was made using extended Hückel calculations[50] carried out on its DFT-optimized geometry using the CACAO program.[51] The computation of the electron localization function (ELF) was done using the ADF-utility program DENSF and visualized with the ADF-GUI module.[38] The chemical bonding of the studied complexes was examined by the Nalewajski−Mrozek bond order method[30] implemented in the ADF program.[38]

■ ASSOCIATED CONTENT

Supporting Information

X-ray crystallographic files for **2**, **3**, and **5** in CIF format. The DFT computed energies of the HOMO and LUMO (eV), HOMO LUMO gaps (ΔE, eV) and selected metric parameters and bond multiplicities for the clusters **1**−**7**. This material is available free of charge via the Internet at http://pubs.acs.org.

■ AUTHOR INFORMATION

Corresponding Author

*E-mail: sghosh@iitm.ac.in (S.G.), halet@univ-rennes1.fr (J.-F.H.).

Notes

The authors declare no competing financial interest.

■ ACKNOWLEDGMENTS

Generous support of the Indo-French Centre for the Promotion of Advanced Research (IFCPAR-CEFIPRA), No. 4405-1, New Delhi is gratefully acknowledged. K.G. thanks the Council of Scientific and Industrial Research (CSIR), New Delhi, for a Senior Research Fellowship. We thank V. Ramkumar for X-ray crystallography analysis.

■ REFERENCES

(1) *The Borane, Carborane, Carbocation Continuum*; Casanova, J., Ed.; Wiley: New York, 1998.

(2) *Inorganometallic Chemistry*; Fehlner, T. P., Ed.; Plenum: New York, 1992.

(3) Gilbert, K. B.; Boocock, S. K.; Shore, S. G. In *Comprehensive Organometallic Chemistry*; Wilkinson, G., Stone, F. G. A., Abel, E. W., Eds.; Pergamon: New York, 1982; Vol. *6*, pp 879−945.

(4) (a) Kennedy, J. D. *Prog. Inorg. Chem.* **1984**, *32*, 519−679. (b) Kennedy, J. D. *Prog. Inorg. Chem.* **1986**, *34*, 211−434.

(5) Barton, L.; Srivastava, D. K. In *Comprehensive Organometallic Chemistry II*; Wilkinson, G., Abel, E. W., Stone, F. G. A., Eds.; Pergamon: New York, 1995; Vol. *I*, Chapter 8, pp 275−373.

(6) Fehlner, T. P. *Organometallics* **2000**, *19*, 2643−2651.

(7) Wade, K. *Adv. Inorg. Chem. Radiochem.* **1976**, *18*, 1−66.

(8) Mingos, D. M. P.; Wales, D. J. *Introduction to Cluster Chemistry*; Prentice Hall: New York, 1990.

(9) Bose, S. K.; Geetharani, K.; Varghese, B.; Mobin, S. M.; Ghosh, S. *Chem.—Eur. J.* **2008**, *14*, 9058−9064.

(10) Bose, S. K.; Geetharani, K.; Ramkumar, V.; Mobin, S. M.; Ghosh, S. *Chem.—Eur. J.* **2009**, *15*, 13483−13490.

(11) (a) Sahoo, S.; Dhayal, R. S.; Varghese, B.; Ghosh, S. *Organometallics* **2009**, *28*, 1586−1589. (b) Bose, S. K.; Geetharani, K.; Varghese, B.; Ghosh, S. *Inorg. Chem.* **2010**, *49*, 6375−6377.

(12) (a) Geetharani, K.; Bose, S. K.; Varghese, B.; Ghosh, S. *Chem.—Eur. J.* **2010**, *16*, 11357−11366. (b) Geetharani, K.; Bose, S. K.; Sahoo, S.; Ghosh, S. *Angew. Chem., Int. Ed.* **2011**, *50*, 3908−3911. (c) Bose, S. K.; Geetharani, K.; Varghese, B.; Ghosh, S. *Inorg. Chem.* **2011**, *50*, 2445−2449. (d) Bose, S. K.; Ghosh, S. *Organometallics* **2011**, *30*, 4788−4791. (e) Dhayal, R. S.; Chakrahari, K. K. V.; Varghese, B.; Mobin, S. M.; Ghosh, S. *Inorg. Chem.* **2010**, *49*, 7741−7747. (f) Sahoo, S.; Mobin, S. M.; Ghosh, S. *J. Organomet. Chem.* **2010**, *695*, 945−949. (g) Geetharani, K.; Tussupbayev, S.; Borowka, J.; Holthausen, M. C.; Ghosh, S. *Chem.—Eur. J.* **2012**, *18*, 8482−8489.

(13) Geetharani, K.; Bose, S. K.; Sahoo, S.; Varghese, B.; Mobin, S. M.; Ghosh, S. *Inorg. Chem.* **2011**, *50*, 5824−5832.

(14) (a) Le Guennic, B.; Jiao, H.; Kahlal, S.; Saillard, J.-Y.; Halet, J.-F.; Ghosh, S.; Shang, M.; Beatty, A. M.; Rheingold, A. L.; Fehlner, T. P. *J. Am. Chem. Soc.* **2004**, *126*, 3203−3217. (b) Krishnamoorthy, B. S.; Kahlal, S.; Le Guennic, B.; Saillard, J.-Y.; Ghosh, S.; Halet, J.-F. *Solid State Sci.* **2012**, DOI: 10.1016/j.solidstatesciences.2012.03.026.

(15) Bose, S. K.; Ghosh, S.; Noll, B. C.; Halet, J.-F.; Saillard, J.-Y.; Vega, A. *Organometallics* **2007**, *26*, 5377−5385.

(16) Onak, T. P.; Williams, R. E. *Inorg. Chem.* **1994**, *33*, 5471−5476.

(17) Bühl, M.; Schleyer, P. v. R. In *Electron Deficient Boron and Carbon Clusters*; Olah, G. A., Wade, K., Williams, R. E., Eds.; Wiley: New York, 1991; Chapter 4, pp 113−142.

(18) (a) King, R. B. *Inorg. Chem.* **2006**, *45*, 8211−8216. (b) King, R. B.; Ghosh, S. *Theor. Chem. Acc.* **2012**, *131*, 1087−1094.

(19) (a) Wade, K. *Inorg. Nucl. Chem. Lett.* **1972**, *8*, 559−562. (b) Mingos, D. M. P. *Nature (London) Phys. Sci.* **1972**, *236*, 99−102. (c) Mingos, D. M. P. *Acc. Chem. Res.* **1984**, *17*, 311−319.
(20) Corbett, J. D. *Struct. Bonding (Berlin)* **1997**, *87*, 157−193.
(21) Aldridge, S.; Hashimoto, H.; Shang, M.; Fehlner, T. P. *Chem. Commun.* **1998**, 207−208.
(22) Belmonte, P. A.; Schrock, R. R.; Day, C. S. *J. Am. Chem. Soc.* **1982**, *104*, 3082−3089.
(23) (a) Churchill, M. R.; Wasserman, H. J. *Inorg. Chem.* **1982**, *21*, 226−230. (b) Campbell, G. C.; Canich, J. A. M.; Cotton, F. A.; Duraj, S. A.; Haw, J. F. *Inorg. Chem.* **1986**, *25*, 287−290. (c) Belmonte, P. A.; Cloke, F. G. N.; Schrock, R. R. *J. Am. Chem. Soc.* **1983**, *105*, 2643−2650.
(24) (a) Churchill, M. R.; Julis, S. A. *Inorg. Chem.* **1977**, *16*, 1488−1494. (b) Churchill, M. R.; Ni, S. W.-Y. *J. Am. Chem. Soc.* **1973**, *95*, 2150−2155.
(25) Bose, S. K.; Geetharani, K.; Sahoo, S.; Reddy, K. H. K.; Varghese, B.; Jemmis, E. D.; Ghosh, S. *Inorg. Chem.* **2011**, *50*, 9414−9422.
(26) Hoffmann, R.; Schleyer, P. v. R.; Schaefer, H. F., III *Angew. Chem., Int. Ed.* **2008**, *47*, 7164−7167.
(27) (a) Becke, A. D.; Edgecombe, K. E. *J. Chem. Phys.* **1990**, *92*, 5397. (b) Silvi, B.; Savin, A. *Nature* **1994**, *371*, 683−686. (c) Savin, A.; Nesper, R.; Wengert, S.; Fässler, T. F. *Angew. Chem., Int. Ed. Engl.* **1997**, *36*, 1808−1832.
(28) Llusar, R.; Beltrán, A.; Andrés, J.; Fuster, F.; Silvi, B. *J. Phys. Chem. A* **2001**, *105*, 9460−9466.
(29) Scioly, A. J.; Luetkens, M. L., Jr.; Wilson, R. B.; Huffman, J. C.; Sattelberger, A. P. *Polyhedron* **1987**, *6*, 741−757.
(30) Nalewajski, R. F.; Mrozek, J. *Int. J. Quantum Chem.* **1994**, *51*, 187−200.
(31) Michalak, A.; DeKock, R. L.; Ziegler, T. *J. Phys. Chem. A* **2008**, *112*, 7256−7263.
(32) (a) Grimes, R. N. In *Metal Interactions with Boron Clusters*; Grimes, R. N., Ed.; Plenum: New York, 1982; pp 269−319. (b) Housecroft, C. E.; Fehlner, T. P. *Adv. Organomet. Chem.* **1982**, *21*, 57−112.
(33) Ring, M. A.; Donnay, J. D. H.; Koski, W. S. *Inorg. Chem.* **1962**, *1*, 109−111.
(34) Besora, M.; Lledós, A. *Struct. Bonding (Berlin)* **2008**, *130*, 149−202.
(35) Ryschkewitsch, G. E.; Nainan, K. C. *Inorg. Synth.* **1975**, *15*, 113−114.
(36) Altomare, A.; Cascarano, G.; Giacovazzo, C.; Guagliardi, A. *J. Appl. Crystallogr.* **1993**, *26*, 343−350.
(37) Sheldrick, G. M. *Acta Crystallogr.* **2008**, *A64*, 112−122.
(38) *ADF2010.02*; SCM, Theoretical Chemistry, Vrije Universiteit: Amsterdam, The Netherlands, http://www.scm.com.
(39) te Velde, G.; Bickelhaupt, F. M.; Baerends, E. J.; van Gisbergen, S. J. A.; Fonseca Guerra, C.; Snijders, J. G.; Ziegler, T. *J. Comput. Chem.* **2001**, *22*, 931−967.
(40) Vosko, S. H.; Wilk, L.; Nusair, M. *Can. J. Phys.* **1980**, *58*, 1200−1211.
(41) (a) Becke, A. D. *J. Chem. Phys.* **1986**, *84*, 4524−4529. (b) Becke, A. D. *Phys. Rev. A* **1988**, *38*, 3098−3100.
(42) Perdew, J. P. *Phys. Rev. B* **1986**, *33*, 8822−8824.
(43) Versluis, L.; Ziegler, T. *J. Chem. Phys.* **1988**, *88*, 322−328.
(44) (a) van Lenthe, E.; Baerends, E. J.; Snijders, J. G. *J. Chem. Phys.* **1993**, *99*, 4597−4610. (b) van Lenthe, E.; Baerends, E. J.; Snijders, J. G. *J. Chem. Phys.* **1994**, *101*, 9783−9792. (c) van Lenthe, E.; van Leeuwen, R.; Baerends, E. J.; Snijders, J. G. *Int. J. Quantum Chem.* **1996**, *57*, 281−293.
(45) (a) Becke, A. D. *Phys. Rev. A* **1988**, *38*, 3098. (b) Lee, C.; Yang, W.; Parr, R. G. *Phys. Rev. B* **1988**, *37*, 785. (c) Becke, A. D. *J. Chem. Phys.* **1993**, *98*, 5648.
(46) del Rosal, I.; Maron, L.; Poteau, R.; Jolibois, F. *Dalton Trans.* **2008**, 3959.
(47) (a) London, F. *J. Phys. Radium* **1937**, *27*, 397−409. (b) Ditchfield, R. *Mol. Phys.* **1974**, *27*, 789−807. (c) Wolinski, K.; Hinton, J. F.; Pulay, P. *J. Am. Chem. Soc.* **1990**, *112*, 8251−8260. (d) Friedrich, K.; Seifert, G.; Grossmann, G. Z. *Phys. D* **1990**, *17*, 45−46.
(48) (a) Schreckenbach, G.; Ziegler, T. *J. Phys. Chem.* **1995**, *99*, 606−611. (b) Schreckenbach, G.; Ziegler, T. *Int. J. Quantum Chem.* **1997**, *61*, 899−918. (c) Schreckenbach, G.; Ziegler, T. *Int. J. Quantum Chem.* **1996**, *60*, 753−766.
(49) (a) Wolff, S. K.; Ziegler, T. *J. Chem. Phys.* **1998**, *109*, 895−905. (b) Wolff, S. K.; Ziegler, T.; van Lenthe, E.; Baerends, E. J. *J. Chem. Phys.* **1999**, *110*, 7689−7698.
(50) Hoffmann, R. *J. Chem. Phys.* **1963**, *39*, 1397−1412.
(51) Mealli, C.; Proserpio, D. M. *J. Chem. Educ.* **1990**, *67*, 399−402.